3

Energy dissipation in large-eddy simulation: dependence on flow structure and effects of eigenvector alignments

Chad Higgins, Marc B. Parlange
Center for Environmental and Applied Fluid Mechanics, and Department of Geography and Environmental Engineering, Johns Hopkins University, Baltimore, USA
and
Charles Meneveau
Center for Environmental and Applied Fluid Mechanics, and Department of Mechanical Engineering, Johns Hopkins University, Baltimore, USA

3.1 Introduction

Most numerical simulations of turbulent flow use grid spacings that far exceed the viscous scale at which turbulent kinetic energy is dissipated into heat. Large-eddy simulation (LES), requires closure models to account for the turbulent motions occurring at small (the so-called subgrid) scales. These motions are responsible for mixing and they interact with the large-scale motions in a way that tends, typically, to transfer kinetic energy to smaller scales in the turbulent energy cascade. This transfer must be reproduced accurately by subgrid-scale (SGS) closures in order to prevent overdamping of resolved scales, or insufficient damping which can lead to spurious instabilities. Lilly (1967) was the first to combine this insight with concepts from the phenomenological theory of 3D turbulence to provide quantitative answers to several important parameterization issues in LES. Our goals in this article are to review briefly Lilly's pioneering contribution, and to reinterpret certain variables using geometric tools.

Forty years ago, Smagorinsky (1963) proposed a simple eddy-viscosity model based on local variables characterizing the motions at the length scale of the computational grid. In this model, the deviatoric part of the SGS stress tensor, τ_{ij}, where

$$\tau_{ij} = \widetilde{u_i u_j} - \tilde{u}_i \tilde{u}_j, \tag{3.1}$$

is set proportional to the strain-rate tensor, $\tilde{S}_{ij} = \frac{1}{2}(\partial_i \tilde{u}_j + \partial_j \tilde{u}_i)$, characterizing the rate of local deformation of the resolved velocity field. In these expressions a tilde denotes spatial filtering at a length scale Δ. The model is written as:

$$\tau_{ij} - \frac{1}{3}\tau_{kk}\delta_{ij} = -2\nu_T \tilde{S}_{ij}. \tag{3.2}$$

The constant of proportionality is the eddy viscosity ν_T which is written as $\nu_T = \lambda^2|\tilde{\mathbf{S}}|$, where $|\tilde{\mathbf{S}}| = (2\tilde{S}_{ij}\tilde{S}_{ij})^{1/2}$. Here λ is a mixing length scale, while $\lambda|\tilde{\mathbf{S}}|$ is a characteristic velocity scale estimated from the shear scale $|\tilde{\mathbf{S}}|$ and the mixing length λ. The mixing length must be chosen judiciously. For locations far from boundaries and in the absence of buoyancy and rotation effects, the only length scale available to characterize the local turbulence structure of the simulated flow is the filter scale, Δ. Dimensionally it follows that $\lambda = c_s\Delta$, where c_s is a dimensionless model parameter. This parameter must be specified in LES, and has been the subject of much attention in the literature (Deardorff, 1971; Mason, 1994; Piomelli, 1999; Meneveau and Katz, 2000).

In Section 3.2, we review Lilly's classic argument linking c_s to the universal Kolmogorov constant c_K. In Section 3.3 we discuss some dependencies between the local SGS dissipation and parameters characterizing the structure of the resolved-scale motions. In particular, we review field experimental data showing that the SGS dissipation is correlated with axisymmetric expanding motions at the resolved scales. In Section 3.4, we present a geometric view of the tensor contraction between SGS stress and strain-rate tensors in terms of the alignment angles among their respective eigenvectors. In Section 3.5, we combine observational evidence about most likely alignment angles among eigenvectors with the expressions for SGS dissipation and, using these empirical inputs, present a prediction of the preferred SGS dissipation as function of the structure parameter of the resolved scales. A discussion is presented in Section 3.6.

3.2 The Smagorinsky–Lilly model parameter

In a ground-breaking paper, Lilly (1967) showed how c_s could be evaluated from basic knowledge of turbulence, and thus c_s is often referred to as the "Smagorinsky–Lilly" constant in the literature. Central to Lilly's development was the realization that the most important effect of the SGS model upon the dynamics of the large-scale structures is the amount of kinetic energy the model extracts. Hence, the energetics of the flow computed in an LES takes on a special role. Lilly (1967) derives the transport equation for the subgrid kinetic energy $E = \frac{1}{2}\tau_{kk}$ and obtains:

$$\frac{\partial E}{\partial t} + \tilde{u}_k\frac{\partial E}{\partial x_k} - \nu\left[\frac{\partial^2 E}{\partial x_k^2} - \widetilde{\left(\frac{\partial u_i}{\partial x_k}\right)^2} + \left(\frac{\partial \tilde{u}_i}{\partial x_k}\right)^2\right]$$
$$= -\tau_{ij}\tilde{S}_{ij} - \frac{\partial}{\partial x_k}\left(\frac{\widetilde{u_k u_i^2}}{2} - \frac{\tilde{u}_k\widetilde{u_i^2}}{2} - \tilde{u}_i\widetilde{u_k u_i} + \tilde{u}_i^2\tilde{u}_k + \frac{\widetilde{u_k p}}{\rho} - \frac{\tilde{u_k}\tilde{p}}{\rho}\right) \quad (3.3)$$

where $\tilde{S}_{ij} = \frac{1}{2}(\partial_j \tilde{u}_i + \partial_i \tilde{u}_j)$. Taking the ensemble average of this equation (denoted below by angled brackets), and assuming steady-state conditions, one obtains the equality of molecular dissipation of SGS kinetic energy and its rate of production:

$$\nu \left[\left\langle \widetilde{\left(\frac{\partial u_i}{\partial x_k} \right)^2} \right\rangle - \left\langle \left(\frac{\partial \tilde{u}_i}{\partial x_k} \right)^2 \right\rangle \right] = -\langle \tau_{ij} \tilde{S}_{ij} \rangle. \tag{3.4}$$

The quantity $-\langle \tau_{ij} \tilde{S}_{ij} \rangle$ is interpreted as the mean flux of kinetic energy from the range of resolved scales into the SGS range, and also appears as a sink in the equation for resolved kinetic energy, $\frac{1}{2}\tilde{u}_k \tilde{u}_k$. When Δ is in the inertial range, the first term in the lhs of (3.4) dominates and equals ε, the overall rate of dissipation by viscosity. Hence, we can write $\varepsilon = -\langle \tau_{ij} \tilde{S}_{ij} \rangle$.

Lilly then makes the next important step in his derivation by replacing τ_{ij} with the Smagorinsky closure. One obtains the expression

$$\varepsilon = 2^{3/2} (c_s \Delta)^2 \langle (\tilde{S}_{ij} \tilde{S}_{ij})^{3/2} \rangle \tag{3.5}$$

as a condition for the Smagorinsky model to extract kinetic energy from the resolved scales at the correct rate. Two more assumptions are required to complete Lilly's original argument: (1) that at the grid scale Δ the turbulence exhibits a universal Kolmogorov spectrum $E(k) = c_K \varepsilon^{2/3} k^{-5/3}$ with turbulence statistics that are isotropic; this assumption is justified when Δ pertains to the inertial range of turbulence; and (2) the third-order statistics of the strain-rate magnitude may be approximated with its second-order moment as

$$\langle (\tilde{S}_{ij} \tilde{S}_{ij})^{3/2} \rangle \approx \langle \tilde{S}_{ij} \tilde{S}_{ij} \rangle^{3/2}. \tag{3.6}$$

The latter assumption is not explicitly stated in Lilly's paper since he did not elaborate explicitly on the nature of statistical averaging underlying the argument. The accuracy of this assumption was recently tested with Direct Numerical Simulation (DNS) data by Cerutti *et al.* (2000) and deviations on the order of 20% were observed in the inertial range (the correction factor β of that paper). Also Novikov (1990) has speculated that small-scale intermittency could introduce a further dependence of c_s upon Δ/l, where l is the integral length scale. Equation (3.6) still leaves the task of evaluating the second-order moment and strain-rate tensor contraction $\langle \tilde{S}_{ij} \tilde{S}_{ij} \rangle$. Using standard techniques from isotropic turbulence analysis, it is straightforward to show that

$$\langle \tilde{S}_{ij} \tilde{S}_{ij} \rangle = \int_0^{\pi/\Delta} k^2 E(k)\, dk \tag{3.7}$$

where, as in Lilly (1967), a spherical spectral sharp filter is used to cut off the

integration in wavenumber space at a wavenumber π/Δ. Substituting this into (3.5) and using the Kolmogorov spectrum $E(k) = c_K \varepsilon^{2/3} k^{-5/3}$ and solving for the coefficient c_s one obtains Lilly's result:

$$c_s = \frac{1}{\pi}\left(\frac{2}{3c_K}\right)^{3/4} \sim 0.165 \text{ (for } c_K = 1.6). \tag{3.8}$$

The analysis has been reproduced in tutorial detail in Pope (2001).

When using computational meshes that are unequal in each Cartesian direction (e.g., $\Delta_1 < \Delta_2 < \Delta_3$), the above derivation can be repeated, but now using an anisotropic 3D filter (Scotti *et al.*, 1993) such as a parallelepiped of sides $2\pi/\Delta_1$, $2\pi/\Delta_2$, and $2\pi/\Delta_3$ in Fourier space. The integrals in Fourier space are more complicated but can be evaluated numerically for exact evaluations of the coefficient. Lilly's central contribution to the Scotti *et al*. (1993) paper was to recognize that the integrations are greatly simplified if an ellipsoidal domain is used in Fourier space instead of a rectangular one. To zeroth order in $\log(a_i)$ (where $a_1 = \Delta_1/\Delta_3$ and $a_2 = \Delta_2/\Delta_3$ are the two grid aspect ratios), one can then show analytically that Δ in the definition of ν_T must be replaced with a length scale based on the cell volume,

$$\Delta_{eq} = (\Delta_1 \Delta_2 \Delta_3)^{1/3}. \tag{3.9}$$

This expression was already proposed on heuristic grounds by Deardorff (1970) and is often used in LES. Lilly's argument published in Scotti *et al.* (1993) thus serves as a formal justification to the often-used cube-root length scale and clearly demonstrates that it is to be preferred over other heuristic proposals that have occasionally been made over the years. For large filter anisotropies, Scotti *et al.* (1993) show that in addition to the use of Δ_{eq}, c_s should be replaced with $c_s f(a_1, a_2)$, where

$$f(a_1, a_2) \approx \cosh\left\{\frac{4}{27}[(\ln a_1)^2 - \ln a_1 \ln a_2 + (\ln a_2)^2]\right\}^{1/2}.$$

The developments above relied upon statistical averaging to define the mean SGS dissipation, $-\langle \tau_{ij} \tilde{S}_{ij} \rangle$. The fact that the average is non-zero is related to subtle relationships among turbulent motions which lead to non-zero correlation among the tensors τ_{ij} and $\tilde{S}_{ij}$. This correlation is a third-order moment (since τ_{ij} is quadratic with velocity and $\tilde{S}_{ij}$ is linear) similar to the third-order velocity structure function that has important dynamic significance. Hence, it is of interest to explore more precisely the nature of these correlations, to which the remaining parts of this chapter are dedicated.

3.3 Field experimental studies of SGS dissipation

Before describing the field experiments, we introduce several variables to be measured from the data. The local SGS dissipation of turbulent kinetic energy is written as $\prod = -\tau_{ij}\tilde{S}_{ij}$. We decompose both the filtered strain rate $\tilde{S}_{ij} = 0.5(\partial_i \tilde{u}_j + \partial_j \tilde{u}_i)$, and the deviatoric SGS stress into their respective eigenvectors and eigenvalues by the transform $A = Q_A \Lambda_A Q_A^{\mathrm{T}}$ where A is an arbitrary symmetric tensor, Q_A is a matrix containing the eigenvectors of A, and Λ_A is a diagonal matrix containing the corresponding eigenvalues of A on its diagonal.

The eigenvalues are named according to their magnitudes as $\alpha \geq \beta \geq \gamma$, and satisfy the condition $\alpha + \beta + \gamma = 0$. This requires $\alpha \geq 0$, $\gamma \leq 0$, and β is either positive or negative. Eigenvectors are named by their corresponding eigenvalues: $\boldsymbol{\alpha}$ is the extensive eigenvector, $\boldsymbol{\gamma}$ is the contractive eigenvector, and $\boldsymbol{\beta}$ is the intermediate eigenvector. To focus attention on the geometric alignment it is of interest to scale out the magnitudes of stress and strain rate and define a dimensionless dissipation, according to

$$\prod^* = \frac{\prod}{|\tilde{\mathbf{S}}||\boldsymbol{\tau}|} = \frac{-\tilde{S}_{ij}\tau_{ij}}{|\tilde{\mathbf{S}}||\boldsymbol{\tau}|}, \tag{3.10}$$

where $|\tilde{\mathbf{S}}| = \sqrt{\tilde{S}_{ij}\tilde{S}_{ij}} = \sqrt{\alpha_{\tilde{S}}^2 + \beta_{\tilde{S}}^2 + \gamma_{\tilde{S}}^2}$ and $|\boldsymbol{\tau}| = \sqrt{\tau_{ij}\tau_{ij}} = \sqrt{\alpha_{-\tau}^2 + \beta_{-\tau}^2 + \gamma_{-\tau}^2}$ (note that henceforth $|\tilde{\mathbf{S}}|$ does not include the factor $\sqrt{2}$ that is usually included in the definition of $|\tilde{\mathbf{S}}|$ for the Smagorinsky model). One can show that $\prod^*$ is now bounded between -1 and 1, and only characterizes the geometric nature of the stress–strain relationship. We now wish to study possible dependencies of this quantity with the geometric structure of the resolved strains. Following Lund and Rogers (1994) we characterize the geometric structure of the resolved strains using the so-called strain state parameter

$$s^* = \frac{-3\sqrt{6}\alpha_{\tilde{S}}\beta_{\tilde{S}}\gamma_{\tilde{S}}}{\left(\alpha_{\tilde{S}}^2 + \beta_{\tilde{S}}^2 + \gamma_{\tilde{S}}^2\right)^{3/2}}. \tag{3.11}$$

The strain state parameter is useful since it indicates the type of motions occurring at the location of the measured filtered strain rate. For example, $s^* = 1$ corresponds to axisymmetric extension (i.e., $\alpha_{\tilde{S}} = \beta_{\tilde{S}} > 0$, $\gamma_{\tilde{S}} < 0$), $s^* = 0$ corresponds to plane strain (i.e., $\beta_{\tilde{S}} = 0$), and $s^* = -1$ corresponds to axisymmetric contraction (i.e., $\alpha_{\tilde{S}} > 0$, $\beta_{\tilde{S}} = \gamma_{\tilde{S}} < 0$). Similar expressions exist to relate the non-dimensional eigenvalues of the SGS stress to the stress state parameter $s_{-\tau}^* = -3\sqrt{6}\alpha_{-\tau}\beta_{-\tau}\gamma_{-\tau}(\alpha_{-\tau}^2 + \beta_{-\tau}^2 + \gamma_{-\tau}^2)^{-3/2}$. The strain state parameter, s^*, is bounded between -1 and 1 for incompressible flow, and the stress state parameter, $s_{-\tau}^*$, is bounded between -1 and 1 when the deviatoric part of the SGS stress $\tau_{ij}^{\mathrm{d}} = \frac{1}{3}\delta_{ij}\tau_{ij}$ is subtracted from each of the diagonal elements of the SGS stress.

Inverse relations also exist (Lund and Rogers, 1994) that express the non-dimensional eigenvalues in terms of the structure parameter:

$$\beta^*_{\tilde{S}} = \frac{\sqrt{6}\beta_{\tilde{S}}}{\sqrt{\alpha^2_{\tilde{S}} + \beta^2_{\tilde{S}} + \gamma^2_{\tilde{S}}}} = 2\cos\left(\frac{5}{3}\pi + \frac{1}{3}\cos^{-1}(s^*)\right),$$

$$\alpha^*_{\tilde{S}} = \frac{\sqrt{6}\alpha_{\tilde{S}}}{\sqrt{\alpha^2_{\tilde{S}} + \beta^2_{\tilde{S}} + \gamma^2_{\tilde{S}}}} = -\cos\left(\frac{5}{3}\pi + \frac{1}{3}\cos^{-1}(s^*)\right) + \sqrt{3}\left|\sin\left(\frac{5}{3}\pi + \frac{1}{3}\cos^{-1}(s^*)\right)\right|,$$

$$\gamma^*_{\tilde{S}} = \frac{\sqrt{6}\gamma_{\tilde{S}}}{\sqrt{\alpha^2_{\tilde{S}} + \beta^2_{\tilde{S}} + \gamma^2_{\tilde{S}}}} = -\cos\left(\frac{5}{3}\pi + \frac{1}{3}\cos^{-1}(s^*)\right) - \sqrt{3}\left|\sin\left(\frac{5}{3}\pi + \frac{1}{3}\cos^{-1}(s^*)\right)\right|. \tag{3.12}$$

Several previous studies of the full three-dimensional structure of SGS dissipation and alignment between the filtered strain-rate tensor and the SGS stress tensor eigendirections have been performed. Tao *et al*. (2002) studied alignments in the turbulent flow in a square duct using holographic particle image velocimetry (HPIV). Higgins *et al*. (2003) studied the flow in the unstable atmospheric boundary layer with arrays of sonic anemometers. Horiuti (2001) used DNS to study alignments. Despite the large disparity in length scales and flow conditions between the studies, they showed strikingly similar qualitative results with preferred orientations of the eigenvectors of $\tilde{S}_{ij}$ and τ_{ij} (see Section 3.4 for further discussion of their results).

In this chapter we present data from the same experimental setup as used in Higgins *et al*. (2003) and discussed in detail in Porté-Agel *et al*. (2001). Two vertically separated horizontal arrays of sonic anemometers were deployed in Davis, California, to obtain spatial measurements of the temperature, T, and the full three-component velocity vector. The upper array contained five sonic anemometers while the lower array contained seven sonic anemometers. Horizontal separations between sonics was 0.4 m and the vertical spacing between the two arrays was 0.51 m. Data were acquired at a temporal resolution of 20 Hz. The friction velocity $u_* = (\langle u'w'\rangle^2 + \langle v'w'\rangle^2)^{1/4}$ and the Monin–Obukhov length $L = \frac{-\langle T\rangle u_*^3}{k\,g\langle T'w'\rangle}$ were used to classify the data into subsets according to the values of z/L, where z is the average height of the sensors above the ground ($z = 3.9$ m). Primes denote fluctuating quantities, $\langle \ldots \rangle$ represents averaging over time, κ is von Kármán's constant ($\kappa = 0.4$) and g is the acceleration of gravity. Atmospheric conditions are classified as having near neutral stability when $|z/L| \leq 0.02$. The friction velocity for the data used was $u_* = 0.27$ m s^{-1}. The present segment represents about 30 minutes of

data and $\sim 40,000$ time realizations, and is distinctly different from the data used in Higgins *et al*. (2003), who used data collected from the convectively unstable atmosphere.

For the direct calculation of the SGS stress, the field measurements are filtered in the spanwise horizontal direction with a box filter, and in the streamwise direction with a Gaussian filter. Taylor's hypothesis is invoked to convert the temporal data record into a streamwise spatial record for streamwise filtering. The filter size, Δ, used throughout the present work corresponds to five times the instrument spacing, i.e., $\Delta \cong 2$ m. For the purposes of this analysis, this scale is considered to fall below the turbulence integral scale (since $\Delta/z < 1$). Spectra shown in Higgins *et al*. (2003) confirm that $\Delta = 2$ m falls broadly within the $k^{-5/3}$ region. No filtering is performed in the vertical direction. For consistency, gradients are calculated with finite differences over a distance of approximately $\Delta/5$ in all three directions. Then $\tilde{S}_{ij}$ and τ_{ij} are computed according to their respective definitions: $\tilde{S}_{ij} = \frac{1}{2}(\partial_j \tilde{u}_i + \partial_i \tilde{u}_j)$, and $\tau_{ij} = \widetilde{u_i u_j} - \tilde{u}_i \tilde{u}_j$. For a complete description of this approximate filtering technique and applications to atmospheric datasets, see Porté-Agel *et al.* (2001), Tong *et al*. (1999), and Horst *et al*. (2004). For applications to wind-tunnel laboratory data from arrays of hot-wire anemometers, see Cerutti and Meneveau (2000), and Kang and Meneveau (2002).

A probability distribution function (PDF) of non-dimensional dissipation for atmospheric sonic anemometer data under near neutral stability is presented in Fig. 3.1. Figure 3.2 shows the conditional PDF of Π^* as function of the parameter

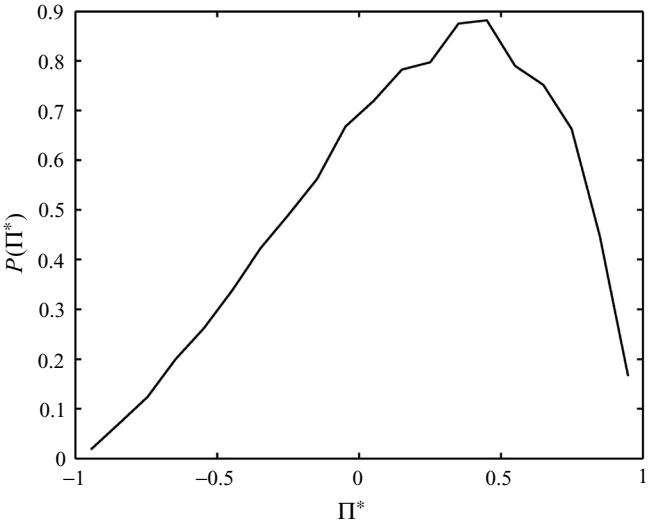

Figure 3.1. PDF of normalized dissipation, Π^*, from the near-neutral atmospheric surface layer. The mean normalized dissipation is positive ($\langle \Pi^* \rangle = 0.2$) and the most likely normalized dissipation is 0.4.

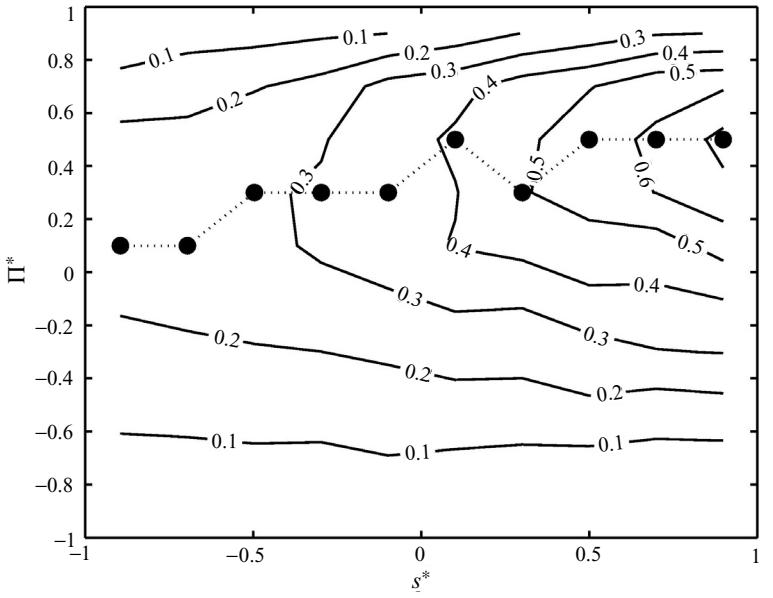

Figure 3.2. Joint PDF of normalized dissipation, Π^*, and strain state parameter. To calculate the joint PDF, the s^* axis was divided into 10 bins and the Π^* axis was divided into 10 bins. The mode normalized dissipation, conditioned on strain state parameter (represented by the symbols and dotted line), tends to increase as s^* increases. Similar trends were shown in Tao *et al.* (2002), but for a different normalization of SGS dissipation.

s^*. Also shown as symbols and dotted line is the mode value of Π^* at given s^*. It shows that the SGS dissipation tends to increase in regions of large s^*, where resolved motions are of the axisymmetric extension type. In the following section we seek to understand this trend in terms of preferred orientations among the two tensors.

Figure 3.3 shows the PDFs of the two structure parameters s^* and $s^*_{-\tau}$ obtained from the present data. Both PDFs peak at $s^* = s^*_{-\tau} = 1$, indicating preferential occurrence of axisymmetric extensional motions, and a preferential axisymmetric contractive stress field. Probability density functions of s^* and $s^*_{-\tau}$ were also presented in both Tao *et al.* (2002) and Higgins *et al.* (2003). Both studies showed that the most likely strain-rate state correspond to $s^* = 1$. A most likely value of $s^* = 1$ was also obtained from DNS of unfiltered turbulence at lower Reynolds numbers and smaller scales by Lund and Rogers (1994) and from multi-component hot-wire data by Tsinober *et al.* (1992). Also in agreement with present results, Tao *et al.* (2002) and Higgins *et al.* (2003) found that the most likely state of the negative SGS stress is $s^*_{-\tau} = 1$. Note that the peak is particularly pronounced for the SGS stress structure, where more than half the data correspond to $s^*_{-\tau} > 0.64$.

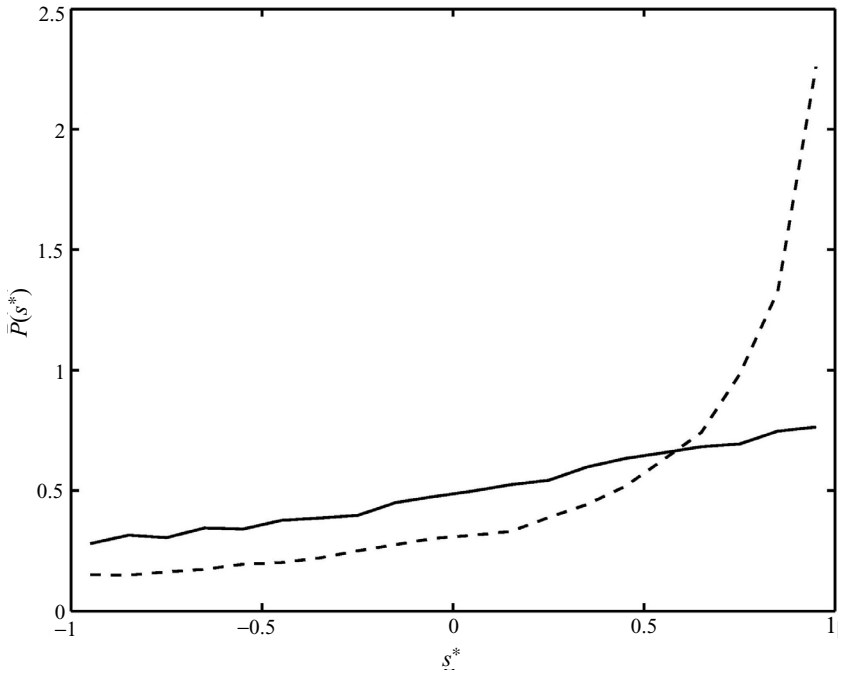

Figure 3.3. PDFs of s^* (solid line) and $s^*_{-\tau}$ (dashed line) showing that both have a most likely value of 1. This indicates that the eigenvectors of both the filtered strain rate, $\tilde{S}_{ij}$, and the negative SGS stress, $-\tau_{ij}$, are in a state of axisymmetric extension. This behavior was already noted in DNS data (Lund and Rogers, 1994), hot-wire anemometer data (Tsinober *et al*., 1992), HPIV data in a square duct (Tao *et al*., 2002) and in the atmospheric surface layer under unstable conditions (Higgins *et al*., 2003).

3.4 Geometric view of stress–strain rate correlation

The contraction of (3.10) can be expanded in terms of the eigenvalues and eigenvectors of the two tensors as follows:

$$\begin{aligned}\Pi = {} & \alpha_{\tilde{S}}\alpha_{-\tau}(\boldsymbol{\alpha}_{\tilde{S}}, \boldsymbol{\alpha}_{-\tau})^2 + \alpha_{\tilde{S}}\beta_{-\tau}(\boldsymbol{\alpha}_{\tilde{S}}, \boldsymbol{\beta}_{-\tau})^2 + \alpha_{\tilde{S}}\gamma_{-\tau}(\boldsymbol{\alpha}_{\tilde{S}}, \boldsymbol{\gamma}_{-\tau})^2 \\ & + \beta_{\tilde{S}}\alpha_{-\tau}(\boldsymbol{\beta}_{\tilde{S}}, \boldsymbol{\alpha}_{-\tau})^2 + \beta_{\tilde{S}}\beta_{-\tau}(\boldsymbol{\beta}_{\tilde{S}}, \boldsymbol{\beta}_{-\tau})^2 + \beta_{\tilde{S}}\gamma_{-\tau}(\boldsymbol{\beta}_{\tilde{S}}, \boldsymbol{\gamma}_{-\tau})^2 \\ & + \gamma_{\tilde{S}}\alpha_{-\tau}(\boldsymbol{\gamma}_{\tilde{S}}, \boldsymbol{\alpha}_{-\tau})^2 + \gamma_{\tilde{S}}\beta_{-\tau}(\boldsymbol{\gamma}_{\tilde{S}}, \boldsymbol{\beta}_{-\tau})^2 + \gamma_{\tilde{S}}\gamma_{-\tau}(\boldsymbol{\gamma}_{\tilde{S}}, \boldsymbol{\gamma}_{-\tau})^2, \quad (3.13)\end{aligned}$$

where $(\boldsymbol{\alpha}, \boldsymbol{\beta})$ denotes the cosine of the angle between two vectors $\boldsymbol{\alpha}$ and $\boldsymbol{\beta}$. Nondimensionalizing with the SGS stress and strain-rate magnitudes yields:

$$\begin{aligned}\Pi^* = {} & \frac{1}{6}[\alpha^*_{\tilde{S}}\alpha^*_{-\tau}(\boldsymbol{\alpha}_{\tilde{S}}, \boldsymbol{\alpha}_{-\tau})^2 + \alpha^*_{\tilde{S}}\beta^*_{-\tau}(\boldsymbol{\alpha}_{\tilde{S}}, \boldsymbol{\beta}_{-\tau})^2 + \alpha^*_{\tilde{S}}\gamma^*_{-\tau}(\boldsymbol{\alpha}_{\tilde{S}}, \boldsymbol{\gamma}_{-\tau})^2 \\ & + \beta^*_{\tilde{S}}\alpha^*_{-\tau}(\boldsymbol{\beta}_{\tilde{S}}, \boldsymbol{\alpha}_{-\tau})^2 + \beta^*_{\tilde{S}}\beta^*_{-\tau}(\boldsymbol{\beta}_{\tilde{S}}, \boldsymbol{\beta}_{-\tau})^2 + \beta^*_{\tilde{S}}\gamma^*_{-\tau}(\boldsymbol{\beta}_{\tilde{S}}, \boldsymbol{\gamma}_{-\tau})^2 \\ & + \gamma^*_{\tilde{S}}\alpha^*_{-\tau}(\boldsymbol{\gamma}_{\tilde{S}}, \boldsymbol{\alpha}_{-\tau})^2 + \gamma^*_{\tilde{S}}\beta^*_{-\tau}(\boldsymbol{\gamma}_{\tilde{S}}, \boldsymbol{\beta}_{-\tau})^2 + \gamma^*_{\tilde{S}}\gamma^*_{-\tau}(\boldsymbol{\gamma}_{\tilde{S}}, \boldsymbol{\gamma}_{-\tau})^2]. \quad (3.14)\end{aligned}$$

Equation (3.14) contains nine distinct angles (inner products) and six eigenvalues. Yet, the alignment between the eigenvectors of two symmetric tensors is fixed with only three Euler angles. Instead of Euler angles, which do not give uniform probability densities when computing their joint probability distributions for random data, we follow the approach of Tao *et al*. (2002) who introduced three specific angles that have uniform measure for random data. To reduce the degrees of freedom in the dissipation equation, we must express each of the nine individual dot products in (3.14) as a function of these three distinct angles. Briefly, the analysis performed by Tao *et al*. (2002) and Higgins *et al.* (2003) fixed the relative orientation between two tensors with a triplet of angles:

$$\theta = \cos^{-1}|(\boldsymbol{\alpha}_{-\tau}, \boldsymbol{\alpha}_{\tilde{S}})|, \phi = \cos^{-1}\left(\left|\left(\boldsymbol{\alpha}^{\mathrm{p}}_{-\tau}, \boldsymbol{\beta}_{\tilde{S}}\right)\right|\left|\boldsymbol{\alpha}^{\mathrm{p}}_{-\tau}\right|^{-1}\right),$$
$$\zeta = \cos^{-1}\left(\left|\left(\boldsymbol{\gamma}^{\mathrm{p}}_{\tilde{S}}, \boldsymbol{\gamma}_{-\tau}\right)\right|\left|\boldsymbol{\gamma}^{\mathrm{p}}_{\tilde{S}}\right|^{-1}\right).$$

Here $\boldsymbol{\alpha}^{\mathrm{p}}_{-\tau}$ is the projection of $\boldsymbol{\alpha}_{-\tau}$ onto the $\boldsymbol{\gamma}_{\tilde{S}} - \boldsymbol{\beta}_{\tilde{S}}$ plane and $\boldsymbol{\gamma}^{\mathrm{p}}_{\tilde{S}}$ is the projection of $\boldsymbol{\gamma}_{\tilde{S}}$ onto the $\boldsymbol{\gamma}_{-\tau} - \boldsymbol{\beta}_{-\tau}$ plane. The angle triplets were calculated for each point in the dataset, and then a 3D joint probability density function of the three angles was computed. By interpreting the modes in the joint PDF, Tao *et al*. (2002), and Higgins *et al*. (2003) were able to deduce the most likely relative orientation of the SGS stress with the filtered strain-rate eigendirections.

To simplify the trigonometry required to express the nine inner products in (3.14) in terms of the three above angles, we circumscribe the set of eigendirections given by the filtered strain rate, and the SGS stress with the unit sphere. Each eigenvector is a unit vector; therefore, each eigenvector can be represented as a point on the unit sphere. The intersection of the sphere and a plane defined by any two eigenvectors forms a great circle that connects the two respective points on the sphere. The arc-length between two points (defined by a great circle) on the unit sphere is identical to the angle between the corresponding vectors. With spherical geometry, the problem is no longer one of finding angles in Cartesian coordinates, but is instead finding distances on the unit sphere. Once this transformation is made, we can use the standard tools of spherical trigonometry to find distances on the sphere. The Law of Cosines for spherical triangles is given by:

$$\cos a = \cos b \cos c + \sin b \sin c \cos A. \tag{3.15}$$

Lower-case letters represent the sides of the spherical triangle and upper-case letters represent the angles opposite of their respective side. The Law of Cosines for spherical triangles will be used to express all of the dot products in (3.14) as functions of the known angle triplet. To complete the final formulation, and to make the geometry as general as possible, it is necessary to redefine the angles

used by Tao *et al*. (2002) and Higgins *et al*. (2003) so that a point can be located anywhere on the sphere relative to an eigenvector coordinate system. We will use the following definitions for the angles:

$$\theta = \cos^{-1}(\boldsymbol{\alpha}_{\tilde{S}}, \boldsymbol{\alpha}_{-\tau}), \tag{3.16}$$

$$\phi = (\boldsymbol{\gamma}_{\tilde{S}} \times \boldsymbol{\beta}_{\tilde{S}}) \cdot \left(\boldsymbol{\alpha}^{\mathrm{p}}_{-\tau} \times \boldsymbol{\alpha}_{\tilde{S}}\right) \cos^{-1} \frac{\left(\boldsymbol{\alpha}^{\mathrm{p}}_{-\tau}, \boldsymbol{\beta}_{\tilde{S}}\right)}{\left|\boldsymbol{\alpha}^{\mathrm{p}}_{-\tau}\right|}, \tag{3.17}$$

$$\zeta = (\boldsymbol{\gamma}_{-\tau} \times \boldsymbol{\beta}_{-\tau}) \cdot \left(\boldsymbol{\gamma}^{\mathrm{p}}_{\tilde{S}} \times \boldsymbol{\beta}_{-\tau}\right) \cos^{-1} \frac{\left(\boldsymbol{\gamma}^{\mathrm{p}}_{\tilde{S}}, \boldsymbol{\gamma}_{-\tau}\right)}{\left|\boldsymbol{\gamma}^{\mathrm{p}}_{\tilde{S}}\right|}. \tag{3.18}$$

The above definitions ensure that the angles are defined relative to a consistent coordinate system, and can vary from $-\pi$ to π. The nine dot products in (3.14) are now given by the following set of equations:

$$(\boldsymbol{\alpha}_{-\tau}, \boldsymbol{\alpha}_{\tilde{S}})^2 = \cos^2\theta, \tag{3.19}$$

$$(\boldsymbol{\gamma}_{\tilde{S}}, \boldsymbol{\alpha}_{-\tau})^2 = \sin^2\theta \sin^2\phi, \tag{3.20}$$

$$(\boldsymbol{\gamma}_{-\tau}, \boldsymbol{\gamma}_{\tilde{S}})^2 = \cos^2\zeta(1 - \sin^2\theta \sin^2\phi), \tag{3.21}$$

$$(\boldsymbol{\gamma}_{-\tau}, \boldsymbol{\alpha}_{\tilde{S}})^2 = \frac{(\cos\theta \sin\phi \cos\zeta + \cos\phi \sin\zeta)^2 \sin^2\theta}{1 - \sin^2\theta \sin^2\phi}, \tag{3.22}$$

$$(\boldsymbol{\beta}_{-\tau}, \boldsymbol{\gamma}_{\tilde{S}})^2 = 1 - (\boldsymbol{\alpha}_{-\tau}, \boldsymbol{\gamma}_{\tilde{S}})^2 - (\boldsymbol{\gamma}_{-\tau}, \boldsymbol{\gamma}_{\tilde{S}})^2, \tag{3.23}$$

$$(\boldsymbol{\beta}_{\tilde{S}}, \boldsymbol{\alpha}_{-\tau})^2 = 1 - (\boldsymbol{\alpha}_{\tilde{S}}, \boldsymbol{\alpha}_{-\tau})^2 - (\boldsymbol{\gamma}_{\tilde{S}}, \boldsymbol{\alpha}_{-\tau})^2, \tag{3.24}$$

$$(\boldsymbol{\beta}_{\tilde{S}}, \boldsymbol{\gamma}_{-\tau})^2 = 1 - (\boldsymbol{\gamma}_{-\tau}, \boldsymbol{\alpha}_{\tilde{S}})^2 - (\boldsymbol{\gamma}_{-\tau}, \boldsymbol{\gamma}_{\tilde{S}})^2, \tag{3.25}$$

$$(\boldsymbol{\beta}_{-\tau}, \boldsymbol{\alpha}_{\tilde{S}})^2 = 1 - (\boldsymbol{\alpha}_{\tilde{S}}, \boldsymbol{\alpha}_{-\tau})^2 - (\boldsymbol{\gamma}_{-\tau}, \boldsymbol{\alpha}_{-\tau})^2, \tag{3.26}$$

$$(\boldsymbol{\beta}_{-\tau}, \boldsymbol{\beta}_{\tilde{S}})^2 = 1 - (\boldsymbol{\beta}_{\tilde{S}}, \boldsymbol{\alpha}_{-\tau})^2 - (\boldsymbol{\beta}_{\tilde{S}}, \boldsymbol{\gamma}_{-\tau})^2. \tag{3.27}$$

Equation (3.14) is first simplified by using the angle relationships in (3.23)–(3.27) (those relationships do not require any predefined angles or geometry) and we are left with

$$\begin{aligned}\Pi^* = \frac{1}{6}[&(\boldsymbol{\alpha}_{\tilde{S}}, \boldsymbol{\alpha}_{-\tau})^2(\alpha^*_{\tilde{S}} - \beta^*_{\tilde{S}})(\alpha^*_{-\tau} - \beta^*_{-\tau}) + (\boldsymbol{\alpha}_{\tilde{S}}, \boldsymbol{\gamma}_{-\tau})^2(\alpha^*_{\tilde{S}} - \beta^*_{\tilde{S}})(\gamma^*_{-\tau} - \beta^*_{-\tau}) \\ &+ (\boldsymbol{\gamma}_{\tilde{S}}, \boldsymbol{\alpha}_{-\tau})^2(\gamma^*_{\tilde{S}} - \beta^*_{\tilde{S}})(\alpha^*_{-\tau} - \beta^*_{-\tau}) + (\boldsymbol{\gamma}_{\tilde{S}}, \boldsymbol{\gamma}_{-\tau})^2(\gamma^*_{\tilde{S}} - \beta^*_{\tilde{S}})(\gamma^*_{-\tau} - \beta^*_{-\tau}) \\ &- 3\,\beta^*_{\tilde{S}}\beta^*_{-\tau}],\end{aligned} \tag{3.28}$$

which will be the starting point of our analysis. To give a complete picture of the final equation form we express all non-dimensional eigenvalues in terms of s^* and

$s^*_{-\tau}$ using the relationships in (3.12), and the angle relations in (3.19)–(3.22):

$$\begin{aligned}\Pi^* = {} & \frac{1}{6}[-3\cos(\Gamma) + \sqrt{3}|\sin(\Gamma)|][-3\cos(\Gamma_\tau) + \sqrt{3}|\sin(\Gamma_\tau)|]\cos^2\theta \\ & + \frac{1}{6}[-3\cos(\Gamma) + \sqrt{3}|\sin(\Gamma)|][-3\cos(\Gamma_\tau) - \sqrt{3}|\sin(\Gamma_\tau)|] \\ & \times \frac{(\cos\theta\sin\phi\cos\zeta + \cos\phi\sin\zeta)^2\sin^2\theta}{1 - \sin^2\theta\sin^2\phi} \\ & + \frac{1}{6}[-3\cos(\Gamma) - \sqrt{3}|\sin(\Gamma)|][-3\cos(\Gamma_\tau) + \sqrt{3}|\sin(\Gamma_\tau)|]\sin^2\theta\sin^2\phi \\ & + \frac{1}{6}[-3\cos(\Gamma) - \sqrt{3}|\sin(\Gamma)|][-3\cos(\Gamma_\tau) - \sqrt{3}|\sin(\Gamma_\tau)|] \\ & \times \cos^2\zeta(1 - \sin^2\theta\sin^2\phi) - 12\cos\Gamma\cos\Gamma_\tau, \end{aligned} \tag{3.29}$$

where $\Gamma = \frac{5}{3}\pi - \frac{1}{3}\cos^{-1} s^*$ and $\Gamma_\tau = \frac{5}{3}\pi - \frac{1}{3}\cos^{-1} s^*_{-\tau}$. Equation (3.29) can be used to investigate the effect of alignment and stress/strain state on dissipation; however, for simplicity, (3.28) is a more natural starting point.

Recall that by definition $\alpha \geq \beta \geq \gamma$. This set of inequalities allows us to determine the signs of the terms containing angles in (3.28):

$$\begin{aligned} (\boldsymbol{\alpha}_{\tilde{S}}, \boldsymbol{\alpha}_{-\tau})^2(\alpha^*_{\tilde{S}} - \beta^*_{\tilde{S}})(\alpha^*_{-\tau} - \beta^*_{-\tau}) &\geq 0 \\ (\boldsymbol{\alpha}_{\tilde{S}}, \boldsymbol{\gamma}_{-\tau})^2(\alpha^*_{\tilde{S}} - \beta^*_{\tilde{S}})(\gamma^*_{-\tau} - \beta^*_{-\tau}) &\leq 0 \\ (\boldsymbol{\gamma}_{\tilde{S}}, \boldsymbol{\alpha}_{-\tau})^2(\gamma^*_{\tilde{S}} - \beta^*_{\tilde{S}})(\alpha^*_{-\tau} - \beta^*_{-\tau}) &\leq 0 \\ (\boldsymbol{\gamma}_{\tilde{S}}, \boldsymbol{\gamma}_{-\tau})^2(\gamma^*_{\tilde{S}} - \beta^*_{\tilde{S}})(\gamma^*_{-\tau} - \beta^*_{-\tau}) &\geq 0. \end{aligned} \tag{3.30}$$

With these constraints, we can deduce alignments of filtered strain-rate and SGS stress eigendirections that maximize or minimize energy dissipation for all possible stress/strain states (s^* and $s^*_{-\tau}$). Eliminating negative terms $(\boldsymbol{\alpha}_{\tilde{S}}, \boldsymbol{\gamma}_{-\tau}) = (\boldsymbol{\gamma}_{\tilde{S}}, \boldsymbol{\alpha}_{-\tau}) = 0$ and maximizing positive terms $(\boldsymbol{\alpha}_{\tilde{S}}, \boldsymbol{\alpha}_{-\tau}) = (\boldsymbol{\gamma}_{\tilde{S}}, \boldsymbol{\gamma}_{-\tau}) = 1$ will yield a maximum dissipation for all possible states of the stress or strain. This maximum is of course attained by the alignment corresponding to the eddy-viscosity model (see Fig. 3.5(a)). The resulting normalized dissipation is given by:

$$\Pi^* = \frac{1}{6}(\alpha^*_{\tilde{S}}\alpha^*_{-\tau} + \beta^*_{\tilde{S}}\beta^*_{-\tau} + \gamma^*_{\tilde{S}}\gamma^*_{-\tau}) = \cos\Gamma\cos\Gamma_\tau + |\sin\Gamma\sin\Gamma_\tau|. \tag{3.31}$$

Equation (3.31) represents an eddy-viscosity behavior, $\Pi^* = 1$, only when $\Gamma_\tau = \Gamma$ (i.e., the stress state and strain state parameters are equal). A plot of the maximum dissipation for all stress–strain state combinations is shown as the upper surface in Fig. 3.4. The short thick line on the upper surface in Fig. 3.4 represents the eddy-viscosity model.

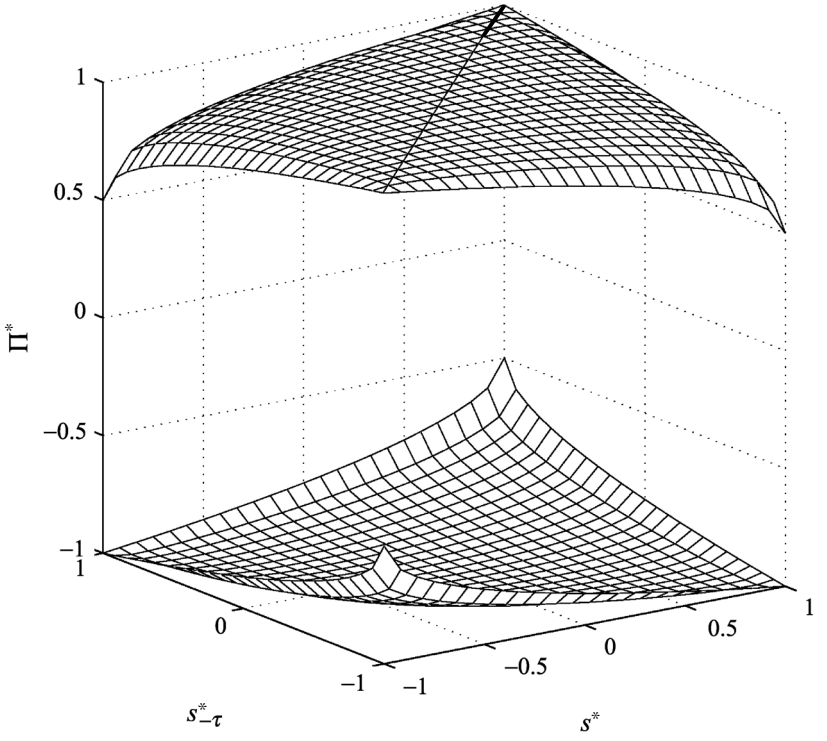

Figure 3.4. Upper and lower bounds on normalized dissipation for each strain state and SGS stress state combination as deduced from (3.28). The short thick line at the upper surface corresponds to the eddy-viscosity closure. This line is also the global maximum of dissipation.

diagonal

Note that the alignment that produces a minimum bound on the normalized dissipation for all SGS stress states and strain states can also be deduced from (3.28). If an alignment is chosen so that the positive terms are eliminated, i.e., $(\boldsymbol{\alpha}_{\tilde{S}}, \boldsymbol{\alpha}_{-\tau}) = (\boldsymbol{\gamma}_{\tilde{S}}, \boldsymbol{\gamma}_{-\tau}) = 0$, and the negatives are maximized, i.e., $(\boldsymbol{\alpha}_{\tilde{S}}, \boldsymbol{\gamma}_{-\tau}) = (\boldsymbol{\gamma}_{\tilde{S}}, \boldsymbol{\alpha}_{-\tau}) = 1$, we will have set the lower bound on dissipation for all possible SGS stress and strain state combinations. The alignment that yields this minimum is when the contractive direction of the filtered strain-rate tensor, $\boldsymbol{\gamma}_{\tilde{S}}$, is aligned with the extensive direction of the (negative) SGS stress tensor, $\boldsymbol{\alpha}_{-\tau}$, and the two intermediate eigendirections are aligned. An interpretive sketch of this alignment is presented in Fig. 3.5(b). Such an alignment yields a normalized dissipation given by:

$$\Pi^* = \frac{1}{6}(\alpha^*_{\tilde{S}}\gamma^*_{-\tau} + \beta^*_{\tilde{S}}\beta^*_{-\tau} + \gamma^*_{\tilde{S}}\alpha^*_{-\tau}) = \cos\Gamma\cos\Gamma_\tau - |\sin\Gamma\sin\Gamma_\tau| \quad (3.32)$$

which is the minimum for all possible stress–strain state combinations. A plot of this minimum is presented as the lower surface in Fig. 3.4.

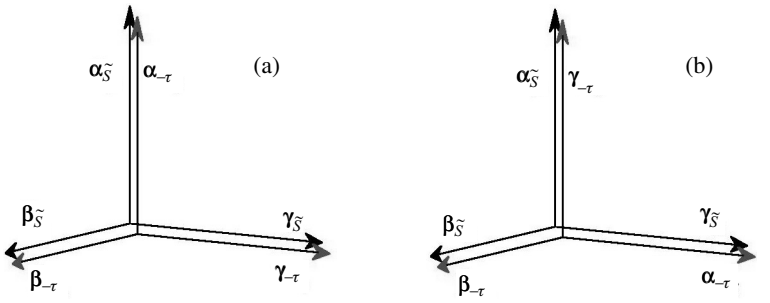

Figure 3.5. Interpretive sketches that give rise to (a) maximum and (b) minimum dissipation. The maximum dissipation is achieved when the vector alignment implied by the eddy-viscosity model is realized (a). The minimum dissipation is achieved by keeping the intermediate eigendirections aligned and pairing extensive and contracting directions together (b). Global minimization of the dissipation function also requires that a functional relationship between strain state and SGS stress state be specified. The global maximum dissipation occurs when the eigenvectors are aligned as in (a) and $s^* = s^*_{-\tau}$. This is achieved when $\tau_{ij} = -\lambda \tilde{S}_{ij}$. The global minimum occurs when the eigenvectors are aligned as in (b) and $s^* = -s^*_{-\tau}$. This is achieved when $\tau_{ij} = \lambda \tilde{S}_{ij}$.

The form of (3.28) can be further simplified if either the filtered strain rate or the SGS stress exhibits axisymmetric contraction or extension. For example, in the most likely case of axisymmetric extension in the filtered strain rate, $s^* = 1$, the non-dimensional eigenvalues have the property $\alpha^*_{\tilde{S}} = \beta^*_{\tilde{S}}$. Two of the required angles then drop from (3.28). When the tensor's eigenvector composition is axisymmetric, all of the directional information is described by the axis of symmetry, including the dissipation.

3.5 Dissipation from observed alignments

Tao *et al.* (2002) and Higgins *et al.* (2003) found two relative orientations of the filtered strain rate and the SGS stress that are highly likely. The two alignments that these studies reported are shown in Fig. 3.6. The atmospheric data used in our study did not contain sufficient points to allow us to obtain statistically converged joint PDFs of the three angles and so we rely on these earlier results. The alignment configuration of Fig. 3.6(a) represents the primary configuration, while the alignment in Fig. 3.6(b) represents the secondary configuration. Each corresponds to a unique alignment of the eigenvectors, but in both alignment configurations, the angle between the two contracting directions (the angle between $\boldsymbol{\gamma}_{\tilde{S}}$ and $\boldsymbol{\gamma}_{-\tau}$) is approximately the same (about 30°), and the contracting direction $\boldsymbol{\gamma}_{-\tau}$ is perpendicular to the intermediate direction of the filtered strain rate, $\boldsymbol{\beta}_{\tilde{S}}$.

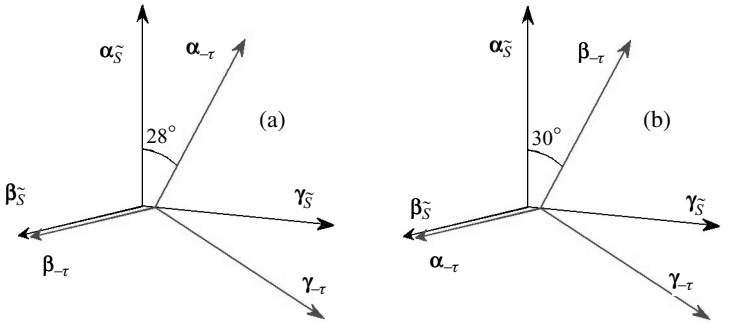

Figure 3.6. (a) Primary and (b) secondary alignment configurations between the filtered strain rate and the SGS stress reported by Tao *et al*. (2002) and Higgins *et al*. (2003). The alignments reflect a bimodal behavior with a characteristic angle between the contracting directions of approximately 30°.

In (3.29), the only variable composed of purely filtered scale quantities is the strain state parameter s^*. Therefore, to explore the dependence of dissipation on filtered scale quantities, we must choose an eigenvector alignment and a value for the SGS stress state parameter.

We have seen that $s^*_{-\tau} = 1$ is the most likely value of this parameter. Using $s^*_{-\tau} = 1$, only the alignment of the axis of symmetry, $\boldsymbol{\gamma}_{-\tau}$, with the filtered strain rate is needed to completely specify the alignment of the filtered strain rate and the SGS stress tensor. This will require only two distinct angles. As mentioned before, it was found in Tao *et al*. (2002) and Higgins *et al*. (2003) that $\boldsymbol{\gamma}_{-\tau}$ is perpendicular to $\boldsymbol{\beta}_{\tilde{S}}$ in both of the likely alignment configurations. Substituting these two conditions into (3.28) ($s^*_{-\tau} = 1$ and $\boldsymbol{\gamma}_{-\tau} \perp \boldsymbol{\beta}_{\tilde{S}}$), and using (3.25), the normalized dissipation becomes

$$\Pi^* = \frac{1}{2}[(\boldsymbol{\gamma}_{\tilde{S}}, \boldsymbol{\gamma}_{-\tau})^2(\alpha^*_{\tilde{S}} - \gamma^*_{\tilde{S}}) - \alpha^*_{\tilde{S}}], \tag{3.33}$$

which is a function of a single angle, namely the angle $(\boldsymbol{\gamma}_{\tilde{S}}, \boldsymbol{\gamma}_{-\tau})$ that is approximately the same in both peaks of the alignment PDF. We can then use the most likely value of this angle as observed from data $(\boldsymbol{\gamma}_{\tilde{S}}, \boldsymbol{\gamma}_{-\tau})^2 \approx \cos^2 30^\circ = 0.75$ (the value reported by Higgins *et al*., 2003). Equation (3.33) then reduces to:

$$\Pi^* = 0.25\left\{2.0\cos\left[\frac{5}{3}\pi - \frac{1}{3}\cos^{-1}(s^*)\right] + \sqrt{3}\left|\sin\left[\frac{5}{3}\pi - \frac{1}{3}\cos^{-1}(s^*)\right]\right|\right\}. \tag{3.34}$$

The value of Π^* therefore varies in a range between about 0.125 when $s^* = -1$ to about 0.625 when $s^* = 1$.

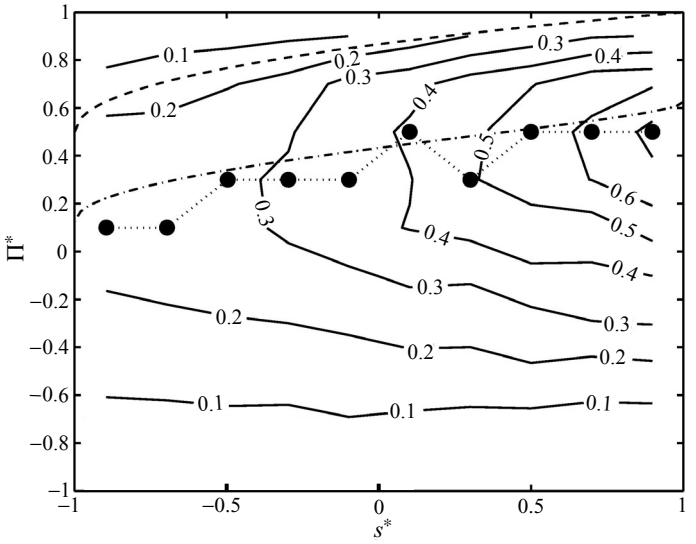

Figure 3.7. Contour plot of the joint PDF between normalized dissipation, Π^*, and the strain state parameter (solid black lines). Symbols and dotted line: the measured mode dissipation as a function of s^* (same as in Fig. 3.2). Dashed line: prediction using $s^*_{-\tau} = 1$ and the eddy-viscosity alignment. Dash–dot line: present prediction using $s^*_{-\tau} = 1$, $\boldsymbol{\gamma}_{-\tau} \perp \boldsymbol{\beta}_{\tilde{S}}$, and $\zeta = 30^\circ$, showing good agreement with the data.

The dash–dot line in Fig. 3.7 denotes the prediction based on the three above assumptions [Equation (3.34)], and is compared to the mode values measured from the data (symbols and dotted line, same as Fig. 3.2).

Picking larger values for $(\boldsymbol{\gamma}_{\tilde{S}}, \boldsymbol{\gamma}_{-\tau})^2$ moves the alignment closer to the one presumed by the eddy-viscosity model. Specifically, for $s^*_{-\tau} = 1$, the prediction for perfect alignment (Fig. 3.5(a)) is shown as a dashed line (this is equal to the upper surface shown in Fig. 3.4 along the line $s^*_{-\tau} = 1$). In addition, the Smagorinsky model gives a constant prediction, $\Pi^* = 1$, for all values of s^* which represents an even greater over-prediction of dissipation. Implications of these observations in terms of improved subgrid models will be discussed in the next section.

3.6 Discussion and conclusions

In this chapter we have reviewed Lilly's ground-breaking development in LES, which recognized the central importance of the SGS dissipation, or contraction between the SGS stress and resolved strain-rate tensors. The original work focused upon the ensemble average value of the SGS dissipation as a means of deriving the model parameter for the Smagorinsky model. We remark in passing that Lilly's

reasoning was extended to more complicated systems, for instance to account for buoyancy (Deardorff, 1971), or viscous effects (Voke, 1996). Another extension was proposed in Cerutti *et al*. (2000) in which the dissipation of enstrophy rather than kinetic energy was shown to be useful to quantify model parameters for hyper-viscosity models.

We have analyzed field experiment data collected under near-neutral conditions, and found that the local SGS dissipation tends to increase in regions of axisymmetric extension. In examining more closely the stress–strain alignments, we have written down an expression for the non-dimensional form of the SGS dissipation. It depends on only five independent parameters (three angles and two non-dimensional structure parameters). The expression allows the investigation of dissipation caused by a particular alignment and stress/strain state configurations (i.e., the local state of the flow). Alignments of eigendirections that give nontrivial limits on dissipation were deduced for every possible stress–strain state.

Using three observations (obtained by inspection of the data and knowledge of the alignment structure presented in Fig. 3.6) the behavior of the normalized dissipation with respect to the strain state is well reproduced. Specifically, the results from Section 3.5 imply that any attempt to reduce the dissipation estimated by the Smagorinsky model with an adjustment to the eddy-viscosity coefficient will have no effect. Recall from Section 3.4 that the eddy-viscosity model gives $\prod^* = 1$ by definition. This is a result of the local non-dimensionalization that scales out tensor magnitudes. The difference in dissipation seen here (Fig. 3.7) from that given by the Smagorinsky model is a result of structural differences in the SGS stress and the filtered strain rate only. If we wished to modify the Smagorinsky model so that it better reproduced the measurements, we would have to modify model structure through either: (1) the eigenvector alignments with a rotation matrix; or (2) by modifying the strain state, s^*, within the strain-rate eigensystem. The former is quite complicated but has the potential to produce the desired result. The latter is simpler, but the reduction in dissipation is limited to the upper surface in Fig. 3.4. Thus, it seems that manipulating the local state of strain alone cannot achieve a great enough reduction in modeled dissipation to match the measured dissipation behavior as a function of s^*. The results show the potential of interpreting turbulent parameters within a geometric framework, and make a clear and immediate connection between the local flow structure and the resulting dissipation.

Acknowledgements

It is with great pleasure that we dedicate this chapter to Professor Douglas K. Lilly. He has been a true pioneer in many areas of geophysical fluid mechanics, and in the area of LES of turbulent flows in particular. We thank F. Porté-Agel, W.E. Eichenger

and M. Pahlow for their efforts in data collection and acknowledge the financial support of NSF-ATM 01300766 and EPA STAR Fellowship.

References

Cerutti, S., Meneveau, C. and Knio, O. M. (2000). Spectral and hyper eddy viscosity in high-Reynolds-number turbulence. *J. Fluid Mech.*, **421**, 307–338.

Cerutti, S. and Meneveau, C. (2000). Statistics of filtered velocity in grid and wake turbulence. *Phys. Fluids*, **12**, 1142–1165.

Deardorff, J. W. (1970). A numerical simulation of 3-dimensional turbulent channel flow at large Reynolds numbers. *J. Fluid Mech*., **41**, 473.

(1971). On the magnitude of the subgrid-scale eddy coefficient. *J. Comp. Phys*., **7**(1), 120–133.

Higgins, C. W., Parlange, M. B. and Meneveau, C. (2003). Alignment trends of velocity gradients and subgrid-scale fluxes in the turbulent atmospheric boundary layer. *Boundary-Layer Meteorol.*, **109**(1), 59–83.

Horiuti, K. (2001). Alignment of eigenvectors for strain rate and subgrid-scale stress tensors. In *Direct and Large Eddy Simulation IV*, B. J. Geurts, R. Friedrich and O. Métais, eds. Kluwer Academic Publishers, 67–72.

Horst, T. W., Kleissl, J., Lenschow, D. H. *et al.* (2003). HATS: Field observations to obtain spatially-filtered turbulence fields from crosswind arrays of sonic anemometers in the atmospheric surface layer. Submitted to *J. Atmos. Sci.*

Kang, H. S. and Meneveau, C. (2002). Universality of large eddy simulation model parameters across a turbulent wake behind a heated cylinder. *J. Turbulence*, **3** 032 (http://jot.iop.org/).

Lilly, D. K. (1967). The representation of small-scale turbulence in numerical simulation experiments. In *Proc. IBM Scientific Computing Symposium on Environmental Sciences, November 14–16, 1966*, Thomas J. Watson Research Center, Yorktown Heights, NY, H. H. Goldstein, ed., IBM Form No. 320–1951, 195–210.

Lund, T. S. and Rogers, M. M. (1994). An improved measure of strain state probability in turbulent flows. *Phys. Fluids*, **6**(5), 1838–1847.

Mason, P. J. (1994). Large eddy simulation: A critical review of the technique. *Quart. J. Roy. Meteor. Soc.*, **120**, 1–26.

Meneveau, C. and Katz, J. (2000). Scale invariance and turbulence models for large-eddy simulation. *Ann. Rev. Fluid Mech*., **319**, 353–385.

Novikov, E. A. (1990). The effects of intermittency on statistical characteristics of turbulence and scale similarity of breakdown coefficients. *Phys Fluids A*, **2**(5), 814–820.

Piomelli, U. (1999). Large eddy simulation: achievements and challenges. *Prog. Aerosp. Sci*., **35**(4), 335–362.

Pope, S. B. (2001). *Turbulent Flows*, Cambridge, UK: Cambridge University Press.

Porté-Agel, F., Parlange, M. B., Meneveau, C., Eichinger, W. E. and Pahlow, M. (2000). Subgrid-scale dissipation in the atmospheric surface layer: Effects of stability and filter dimension. *J. Hydrometeorol.*, **1**, 75–87.

Porté-Agel, F., Parlange, M. B., Meneveau, C. and Eichinger, W. E. (2001). A priori field study of the subgrid-scale heat fluxes and dissipation in the atmospheric surface layer. *J. Atmos. Sci*., **15**, 2673–2697.

Scotti, A., Meneveau, C. and Lilly, D. K. (1993). Generalized Smagorinsky model for anisotropic turbulence. *Phys. Fluids A*, **5**(9), 2306–2308.

Smagorinsky, J. (1963). General circulation experiments with the primitive equations. I. The basic experiment. *Mon. Wea. Rev*., **91**, 99–164.

Tao, B., Katz, J. and Meneveau, C. (2002). Statistical geometry of subgrid-scale stresses determined from holographic particle image velocimetry measurements. *J. Fluid Mech*., **457**, 35–78.

Tong, C., Wyngaard, J. C. and Brasseur, J. G. (1999). Experimental study of the subgrid-scale stresses in the atmospheric surface layer. *J. Atmos. Sci*., **56**, 2277–2292.

Tsinober, A., Kit, E. and Dracos, T. (1992). Experimental investigation of the field of velocity-gradients in turbulent flows. *J. Fluid Mech*., **242**, 169–192.

Voke, P. R. (1996). Subgrid-scale modeling at low mesh Reynolds number. *Theor. Comp. Fluid Dyn*., **8**(2), 131–143.